Sensitivity Analysis of Pine Island Glacier ice flow using ISSM and DAKOTA

E. Larour,[1] J. Schiermeier,[1] E. Rignot,[1,2] H. Seroussi,[1] M. Morlighem,[2] and J. Paden[3]

Received 9 July 2011; revised 15 February 2012; accepted 27 February 2012; published 13 April 2012.

[1] Assessing output errors of ice flow models is a major challenge that needs to be addressed if we are to increase our confidence level in projections of mass balance in Antarctica and Greenland. Major inputs to ice flow models include geometry (ice thickness and surface elevation), constitutive laws and boundary conditions (geothermal flux, basal drag coefficient, surface temperature). These inputs can be either measured, in which case they carry errors due to instruments, or inferred using inverse methods (such as basal drag which is inverted using InSAR surface velocities) in which case they carry additional errors generated by the inversion process itself. In both cases, these input errors will result in uncertainties that propagate throughout a forward model, and that influence output diagnostics. In order to estimate the resulting error margins on diagnostics such as mass flux, we develop a new framework based on the Design Analysis Kit for Optimization and Terascale Applications (DAKOTA), which we interface to the Ice Sheet System Model (ISSM). We present results on the Pine Island Glacier, West Antarctica, for which we evaluate error margins of mass flux across the whole glacier, given currently known error margins on ice thickness, basal friction and ice hardness. Our results suggest errors in these inputs propagate linearly through the ice flow model, providing a way to 1) calibrate measurement requirements for field campaigns collecting data such as bedrock or surface topography 2) quantify uncertainties in projections of mass balance and 3) assess the sensitivity of model outputs to input parameters. This new error propagation model should help quantify confidence levels that we assign to model projections for the mass balance of Antarctica and Greenland, which will ultimately improve our projections of future sea level rise in a warming climate.

Citation: Larour, E., J. Schiermeier, E. Rignot, H. Seroussi, M. Morlighem, and J. Paden (2012), Sensitivity Analysis of Pine Island Glacier ice flow using ISSM and DAKOTA, *J. Geophys. Res.*, *117*, F02009, doi:10.1029/2011JF002146.

1. Introduction

[2] Influx of fresh water from Antarctica and Greenland will soon overtake steric effects as the largest contributor to sea level rise [*Rignot et al.*, 2010; *Velicogna*, 2009]. Understanding the key controls that drive the evolution of the mass balance of these two continents is therefore becoming critical. If we are to accurately project mass balance into the near future, we need to at least understand how sensitive current ice flow models are to input parameters. The goal is to be able to rank each model input in terms of its influence on model outputs (for example, ice flow velocity or temperature) and resulting diagnostics (such as mass flux at the grounding line), and whether our current knowledge of these model inputs is sufficient to significantly reduce errors in projections of mass balance. This type of effort will also inform data collection campaigns such as Operation IceBridge, IceSat-2, GRACE-FO or CryoSat-2, and improve return on science by optimizing flight plans to target areas where model inputs are not sufficiently well known.

[3] The first efforts to understand the main controls on ice sheet flow were carried out by *MacAyeal* [1992, 1993], using control methods. The goal was to invert for the basal drag coefficient on the Siple Coast ice streams, using adjoint-based control methods. Ice flow models used in this type of study were based on the Shelfy-Stream Approximation (SSA) [*Morland*, 1987; *MacAyeal*, 1989], which has the advantage of being self-adjoint in the case of linear viscous flow, or nearly self-adjoint when relying on nonlinear rheology. This advantage was exploited in later studies by *Vieli and Payne* [2003], *Joughin et al.* [2004, 2006], *Larour* [2005], *Vieli et al.* [2006], and *Khazendar et al.* [2007, 2009] to invert for basal drag on various basins of Antarctica and Greenland, as well as ice hardness on various ice shelves in Antarctica. Recent efforts by *Morlighem et al.* [2010] and *Seroussi et al.* [2011] implemented such control methods on

[1]Jet Propulsion Laboratory, California Institute of Technology, Pasadena, California, USA.
[2]Department of Earth System Science, University of California, Irvine, California, USA.
[3]Center for Remote Sensing of Ice Sheets and EECS Department, University of Kansas, Lawrence, Kansas, USA.

0148-0227/12/2011JF002146

higher-order models [*Blatter*, 1995; *Pattyn*, 1996] including full-Stokes [*Stokes*, 1845]. Such control methods are however restricted to the solution of the stress equilibrium equations, used in a forward capability, assuming the thermal regime is held constant. The adjoint state provided in such methods was also never taken advantage of to directly compute sensitivities.

[4] *Heimbach and Bugnion* [2009] were the first to compute the adjoint of a full 3D Ice Sheet Model, the SImulation COde for POLythermal Ice Sheets, SICOPOLIS [*Greve*, 1997a, 1997b], in order to access the sensitivity of the ice sheet volume to variations in several parameters, including the basal drag coefficient and the surface accumulation rate. The approach taken relied on automatic differentiation [*Giering and Kaminski*, 1998; *Utke et al.*, 2008; *Hascoët*, 2004] to compute the adjoint of the ice flow model. This kind of approach is very powerful when the complexity of the model is such that no easy generation of the adjoint is possible. For higher-order models, this type of approach has not successfully been carried out yet except for plan view vertical models such as the model by *Brinkerhoff et al.* [2011]. There are several reasons for that, the main one being the complexity and software challenge it represents. Another reason for ice flow models relying on C/C++, such as the Ice Sheet System Model (ISSM) [*Larour et al.*, 2012], is that automatic differentiation compilers such as OpenAD [*Utke et al.*, 2008] or Tapenade [*Hascoët*, 2004] are not yet able to handle the entire spectrum of C/C++ capabilities such as polymorphism, abstract classes and class derivation.

[5] For such models, the only viable solution so far is based on sampling methods [*Metropolis and Ulam*, 1949; *McKay et al.*, 1979] and local reliability methods [*Haldar and Mahadevan*, 2000]. Historically, sampling methods have been used to explore the input parameter space according to statistical distributions specified for each input parameter. Output diagnostics (such as the Greenland Ice Sheet volume used by *Heimbach and Bugnion* [2009]) are then computed using forward model runs, for each sample of the parameter space that is generated. Statistical output distributions are then computed, and relied upon to assess the sensitivity to input parameters. The obvious disadvantage of this type of method is the computational cost, because the number of samples generated must be statistically representative in spanning the parameter space. The advantage is that this method is robust, and can be used in a flexible way for any type of model, irrespective of the physics involved in the underlying model.

[6] The other approach is based on local reliability methods [*Haldar and Mahadevan*, 2000] which compute finite difference partial derivatives for the output response with respect to each input variable at their baseline values. This type of method requires fewer iterations than sampling methods, and can be used to compute sensitivities efficiently. However, this approach is valid in general for linear problems, or for small perturbations to the system. When large error margins exist on the input parameters, or if the ice flow model is highly non-linear, this type of approach breaks down, and sampling methods are the only robust way to approach sensitivity studies.

[7] Both methods can be used to explore the sensitivity of an ice flow model, in the absence of a viable option to compute the adjoint state. In terms of computation time, the adjoint method is the fastest, as it relies on one forward run of the adjoint model to supply sensitivities of one output diagnostics to any model input, including entire input fields such as ice thickness, ice rigidity or basal drag at the ice/bed interface. Local reliability methods are considerably more time consuming, as one forward run of the model needs to be run for each model input. For field inputs such as thickness, this implies one forward run for each vertex value of the thickness, leading potentially to as many forward runs at there are vertices in the mesh. Finally, sampling analyses are the most time consuming, as they rely on a statistically significant number of forward runs for each model input. Usually, 20–30 samples are needed for each model input, which can be computationally prohibitive.

[8] Here, we present a new integrated model, which merges the ISSM ice flow modeling capabilities with the Design Analysis Kit for Optimization and Terascale Applications (DAKOTA) statistical analysis capabilities. This new model is applied to the Pine Island Glacier (PIG), West Antarctica. Using sampling methods, we determine the uncertainty in mass flux due to errors in ice thickness, propagated throughout a 2D SSA ice flow model. Here, we are not interested in how the model inputs are determined, for example using inverse methods and InSAR surface velocities, but rather, the goal of the study is to assess the forward propagation of errors from model inputs to model diagnostics. We also use local reliability methods to compare the sensitivity of mass flux to three key model inputs: ice thickness, basal drag coefficient and ice hardness. We evaluate the three inputs in terms of their importance in contributing to mass flux errors for the main tributaries of PIG. We also evaluate how localized the sensitivity of mass flux is and how strongly coupled neighboring tributaries are.

[9] The study is structured as follows. In the first part, we describe the new integrated model including the ice flow formulation, sampling and local reliability analyses, as well as mesh partitioning methods. In the second part, we describe the validation of the new model. In the third part, we describe the model setup for Pine Island Glacier, as well as the data sets used. In the fourth part, we present the results of the sampling and local reliability analyses. In the fifth part, we discuss our findings, and its implications for modeling and data collection campaigns. We finally conclude on the significance and perspectives that this new type of study opens up.

2. Model

[10] The sensitivity analyses we carry out on PIG are based on interfacing between a standard 2D ice flow model and the DAKOTA framework. In this section, we describe both components in detail.

2.1. Ice Flow Model

[11] PIG is a fast flowing ice stream, for which velocities reach up to 4500 m/yr at the grounding line [*Rignot*, 2008]. The bulk of the ice flow occurs at velocities greater than 60 m/yr, for which shear stresses are confined mainly near the bed. For this type of ice flow configuration, we use a two-dimensional, vertically-integrated form of the ice flow equations, the Shelfy-Stream Approximation (SSA), based on that by *MacAyeal* [1989, 1992] where most of the ice

flow is due to basal sliding. This model is also applicable for ice shelf flow, where basal friction due to water is taken equal to zero. The system of equations is discretized using the continuous Galerkin Finite Element Method (FEM). This model is simple and computationally efficient, and is implemented within ISSM [*Larour et al.*, 2012; *Morlighem et al.*, 2010; *Seroussi et al.*, 2011]. The model inputs include ice thickness, basal drag coefficient α at the ice/bed interface and ice hardness B. The model outputs (or prognostic variables) include the three components V_x, V_y and V_z of ice flow velocity. The diagnostic of interest in this study is the depth-averaged mass flux across fluxgates, which is computed using the output velocity and ice thickness (see later in this section). Some of the model inputs cannot be measured directly, such as the basal drag coefficient α. The latter is used in a friction law of the following type:

$$\boldsymbol{\tau_b} = -\alpha^2 N \mathbf{v_b} \tag{1}$$

where $\mathbf{v_b}$ is the basal velocity vector tangential to the glacier base plane, N the effective pressure of the water at the glacier base [*Paterson*, 1994], $\boldsymbol{\tau_b}$ the tangential component of the external force $\boldsymbol{\sigma} \cdot \mathbf{n}$, $\mathbf{n}$ the outward pointing normal vector and α the basal drag coefficient. In order to evaluate the effective pressure, a hydrological model is required, which is only a work in progress [*Larour et al.*, 2012]. As a first order approximation, we use $N = \rho g h$ [*Paterson*, 1994], where h is the height of the ice sheet surface above the level at which the ice sheet would lie if it was in hydrostatic equilibrium.

[12] Ice hardness is taken from a Norton-Hoff rheology law [*Glen*, 1955]:

$$\mu = \frac{B}{\dot{\varepsilon}_e^{\frac{n-1}{n}}} \tag{2}$$

where μ is the non-linear ice viscosity, B the ice hardness, n Glen's law coefficient and $\dot{\varepsilon}_e$ the effective strain rate. In order to compute B, which is temperature dependent [*Paterson*, 1994], we rely on a thermal model presented by *Larour et al.* [2012] and *Morlighem et al.* [2010]. The model is run to steady state, and assumes as boundary conditions surface temperatures at the top and geothermal heat flux at the ice/bed interface. At the boundaries of the domain, ice is almost stagnant and reaches almost into the ice divide. We therefore assume that advection of cold ice is negligible. The model captures full 3D advection and conduction in the bulk of the ice and also includes strain induced viscous heating as well as frictional heating at the ice/bed interface. In order to reliably capture the viscous and frictional heating, we couple the thermal model with an inversion of the basal drag coefficient α (see *Morlighem et al.* [2010] for more details), which ensures B is not capturing effects that pertain to the mechanics of friction represented by α.

[13] One of the issues in specifying model inputs for a forward model is the fact that some of the inputs cannot be measured. Here, we are interested in the 2D SSA ice flow model, for which ice thickness is the only measurable model input. Ice hardness B and basal drag coefficient α are difficult to measure on the ground, and they are usually inferred using inverse methods, which themselves depend on a forward model and InSAR surface velocities. Here, our approach is to model B using Glen's flow law and a steady state thermal model, and to invert α using inverse methods. Ice thickness H is observed from data on the ground. This has specific implications for uncertainty analyses. Indeed, specifying errors for α and B is difficult, and is probably outside the scope of the present study, as such errors would have to be inverted from existing observations such as surface velocity and observed temperatures respectively. However, there is extensive observational data to measure ice thickness along with corresponding errors, and the goal of the present study is to use such data to measure the impact on forward propagation of errors in the 2D SSA model. In regards to B and α, we only use them for local reliability methods, where we specify equal error margins for all input parameters. The goal is comparatively assess which model inputs diagnostics are most sensitive to.

[14] As alluded to before, the 2D SSA model can be inverted to infer unknown properties such as basal drag coefficient α from observed InSAR surface velocities [*Morlighem et al.*, 2010; *Larour et al.*, 2012]. Here we use this capability to invert α on the grounded ice, in order to match surface velocities from [*Rignot*, 2008] (Figure 1). The resulting model matches velocities within 10% of observations.

[15] This initial model becomes the basis for our uncertainty analyses, for which we vary first the ice thickness (for sampling analyses) and second ice thickness, ice hardness and basal drag coefficient (for local reliability analyses) and compute corresponding model outputs (ice flow velocity) along with diagnostics, specifically the mass flux through fluxgates that are defined in Figure 1. Thirteen fluxgates are positioned along the main tributaries of PIG, which are used to compute the mass flux M_i for each gate i such that:

$$M_i = \int_{s=0}^{s=L} \rho_{ice} H \boldsymbol{v} \cdot \boldsymbol{n}\, dl \tag{3}$$

where s is the curvilinear coordinate along the curved fluxgate contour, L the overall horizontal length of the fluxgate, ρ_{ice} the density of ice, H the local thickness along the fluxgate, $\boldsymbol{v}$ the depth-averaged horizontal velocity vector, $\boldsymbol{n}$ the local downstream normal to the fluxgate contour, and dl an elementary curvilinear increment.

[16] Mass fluxes through the thirteen gates are computed simultaneously for each forward run, and used as diagnostics to drive uncertainty analyses. In order to capture the mass flux of PIG as realistically as possible, fluxgates 1 and 2 are mapped onto the ice front and grounding line positions in 1996, and the other eleven fluxgates are positioned at the onset of PIG's main tributaries. Mass flux through each one of these gates is used as a metric to estimate the sensitivity of ice flow models on PIG. Indeed, these fluxes capture how much mass is being advected along the tributaries and into the main ice stream, which ultimately controls the mass balance of the whole basin.

2.2. Sampling and Local Reliability Methods Using DAKOTA

[17] We rely on ISSM to propagate errors from model inputs to outputs as well as resulting diagnostics. However, for uncertainty quantification, we rely on the DAKOTA toolkit [*Eldred et al.*, 2008]. This toolkit is integrated with ISSM to drive all forward model runs based on different types of uncertainty analysis strategies. These include

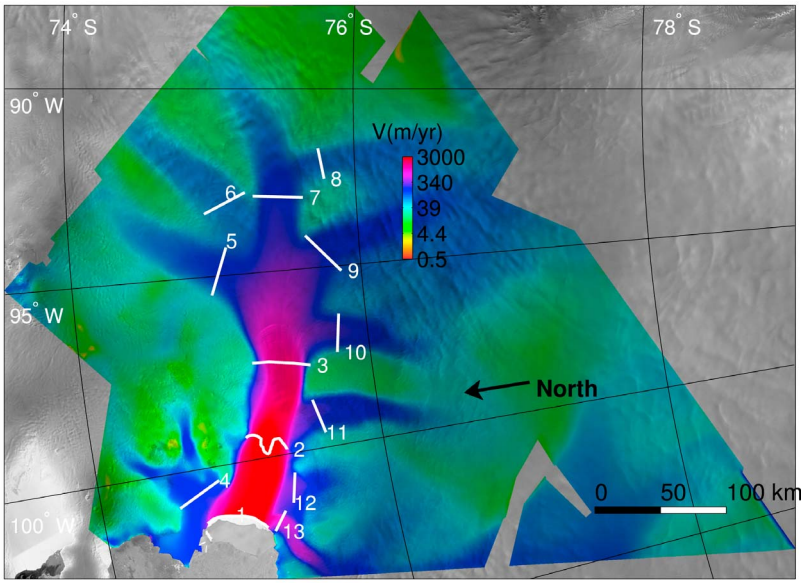

Figure 1. Fluxgates used to compute mass fluxes on tributaries of PIG. Each gate is numbered from 1 to 13, and corresponds to one tributary. Gate 1 coincides with the ice front, and gate 2 coincides with the 1996 grounding line [*Rignot*, 2008]. The gates are superimposed on an InSAR surface velocity map of the area, in logarithmic scale [*Rignot*, 2008].

among others sampling analyses, such as Monte-Carlo [*Metropolis and Ulam*, 1949] and Latin Hypercube [*Iman et al.*, 1981], and local reliability methods for evaluating sensitivities [*Haldar and Mahadevan*, 2000]. Other types of analyses which we are not interested in here include parameter space studies, optimization and design of experiments studies. Sampling analyses are well known techniques to quantify the uncertainty in model diagnostics from errors in model inputs. They are historically used when sensitivities cannot be computed easily for a forward model. Similarly, local reliability methods are used to compute local derivatives of output diagnostics, using a forward model and specified error ranges in model inputs. They integrate error margins into sensitivity analyses in order to enable comparisons between model inputs that may have large errors but low impact on the forward model and on the opposite model inputs with small errors but large impact on the forward model.

[18] For sampling analyses, model inputs are specified within a certain error range Δ_{err}. The type of error determines the statistical distribution used to sample the model input. For example, normal and uniform are among the most typical distributions. These distributions can be fully described by an average μ and standard deviation σ for the normal distribution, and an average μ and radius r or diameter d for the uniform distribution. The way we calibrate μ is straightforward, as the average is essentially the value of the measurement. For σ, we use the fact that within a normal distribution, 99% of the values fall within the interval $[-3\sigma : +3\sigma]$, which yields $\sigma = 1/3\ \Delta_{err}$. For the radius r of a uniform distribution, we just set $r = \Delta_{err}$. In the present study for example, we rely on Ground Penetrating Radar (GPR) measurements of ice thickness. These measurements can be validated using cross-over errors, which are calibrated for each point where two independent measurements are available. The cross-over errors can then be directly used to prescribe σ or r. For ice rigidity B and α, such measurements are not available, and we refrain from attempting to assess the error in such model inputs. Once distributions are prescribed, repeated analyses are run for different values of the input variables generated from the distributions, and statistics are calculated for the output responses. Typically means, standard deviations, and cumulative distribution functions (CDFs) are calculated, even though the output responses need not be (and in general are not) normal distributions.

[19] Generation of the values of the input variables is performed in a number of ways. Probably the most common is traditional Monte Carlo (MC), where the variables are generated randomly according to the specified distributions. This has the disadvantage that values in the tails may be neglected, since those probabilities are very low; however, values in the tails are often critical in the bounds of uncertainty quantification. A second way of generating the input variables is Latin Hypercube Sampling (LHS), which is a binned approach [*Swiler and Wyss*, 2004]. The n-dimensional variable space is divided into equal-probability bins according to the given distributions, such that one and only one sample occurs in each bin. This has the advantage of forcing samples into the tails and is also a more efficient method of sampling for a given level of statistical accuracy. Of course, the LHS method comes with a certain overhead in the computation of the samples as compared to the MC sampling, because of the need to ensure uniqueness of the samples in each bin.

[20] For a large number of input variables, the cost of sampling analyses to decrease the confidence intervals of the output responses to desired levels may be prohibitive, since

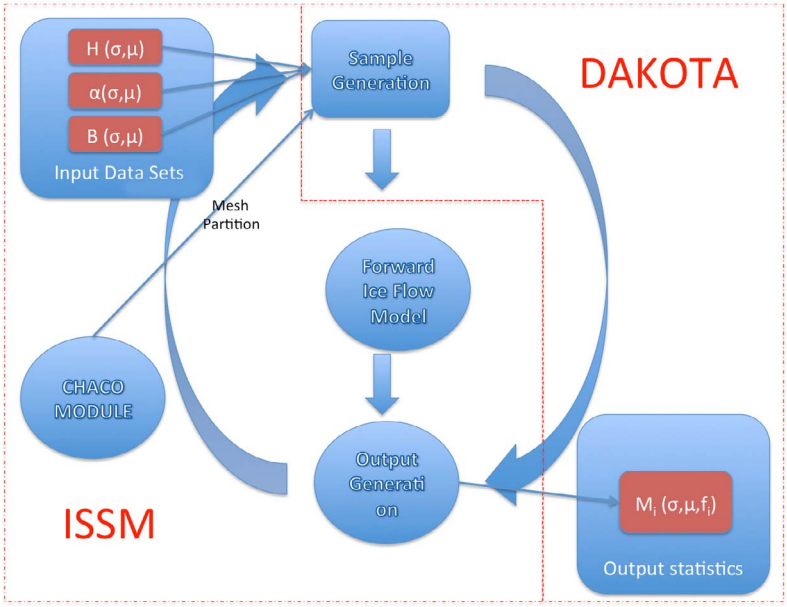

Figure 2. Software architecture of the coupled ISSM-DAKOTA capability, for uncertainty analysis and local reliability analysis, including the CHACO mesh partitioner.

the number of samples required increases geometrically with the number of input variables. In this case, a local reliability analysis may be performed to determine the input variables that have the most significant effects on the output variables. In essence, this method calculates a finite difference partial derivative for each output response with respect to each input variable at their baseline values, which requires only $n + 1$ solutions. The variables that have the largest effects can then be studied further, for example with sampling or parameter methods, and those with little or no effect might not be of interest.

[21] Local reliability methods work best when the problem is linear in the neighborhood of the baseline solution. The finite difference step size is typically defined by the user, so if the function is not linear in the area, the value of the secant will change. If the variable is of primary interest, one-dimensional parameter studies (or different step sizes) can be used to ascertain its behavior. The local reliability method also considers only one variable at a time, but n-dimensional parameter studies can be used to ascertain if any input variables of interest have a coupling effect.

[22] For the local reliability method, given an ice flow model M capable of computing ice velocity V from N model inputs X_i (for example, surface and thickness at each vertex of the mesh), one can assess the value of a response (for example, mass flux through a fluxgate), itself function of the model output V:

$$r = r(V) \text{ with } V = M(X_1, X_2, .., X_N) \tag{4}$$

We can define sensitivities θ_i as:

$$\theta_i = \frac{\partial r}{\partial X_i} \tag{5}$$

[23] The mean of the output responses is assumed from the baseline value. If each of the input variables is independent, the variance σ_r^2 of the output response can be computed from the well-known error propagation equation [*Coleman and Steele*, 1989]:

$$\sigma_r^2 = \sum_{i=1}^{N} \theta_i^2 \cdot \sigma_i^2 \tag{6}$$

where the σ_i^2 are the specified variances of each input variable. Importance factors F_i for each input variable may be calculated by dividing each right-side term of the equation by σ_r^2:

$$F_i = \frac{\theta_i^2 \cdot \sigma_i^2}{\sigma_r^2} \tag{7}$$

These importance factors provide non-dimensional quantities that add up to unity and therefore can be used to rank the contribution of the input variables.

[24] Computation of the importance factors is carried out by DAKOTA. Ice flow modeling is carried out by ISSM. The way both capabilities interact is shown in Figure 2. ISSM deals with processing the input parameters, specifying the nature of the statistical distribution of inputs, and feeding the corresponding characteristics (for example, mean and standard deviation in the case of a normally distributed parameter) to DAKOTA. The latter then generates samples which are fed back to ISSM. Each sample input is then used to update relevant properties of the model. This is straightforward for α and B, which are direct inputs to the model, but less so for thickness H, which controls the position of the bed and surface of the ice . We adopt the following strategy to update the latter: if a vertex is on the ice shelf, then ice thickness is hydrostatically distributed for each update; if a

vertex is on the ice sheet, the bedrock is updated so as to leave the surface of the ice intact. In this study, we are therefore interested in the response of the model to errors in the bed position on the grounded part, and errors in the thickness on the floating part.

[25] Once all updates have been carried out, we run the forward model (here, our 2D SSA ice flow model) to generate outputs (here the mass flux through our fluxgates specified in Figure 1). This process is repeated each time DAKOTA samples the inputs. Once all the runs have been carried out, output statistics are generated by DAKOTA, usually assuming that the output statistical distribution is normal (which may not be the case). In the case of local reliability methods, importance factors are also generated, which are then used to study the sensitivity of model outputs to input parameters.

2.3. Mesh Partitioning

[26] Both the sampling and the local reliability methods are based on updates of input variables, according to their statistical distribution. For a spatially distributed input variable which covers the entire mesh domain, such as the thickness or basal drag coefficient, the domain must be partitioned into a number of discrete regions to be updated. The finite element mesh provides a convenient discretization of the domain; however, varying the input variable for each finite element node or element would be prohibitive for very large problems. In addition, there is the problem of area coverage. For anisotropic meshes where local element areas vary widely, some variables would have an inordinate contribution to the response given the physical areas over which they extend.

[27] For each partition surface, a statistical distribution is specified for the field being sampled. As an example, if thickness is being considered, error margins on thickness measurements from GPR can be used to specify the 3σ standard deviation for that particular partition. Also, the average value of thickness over the partition nodes can be used to specify the mean value of the input variable. Each node of the mesh that belongs to the partition area will behave according to this statistical distribution. Since the thicknesses are specified at the nodes, they will be linear over the elements between the partitions with no discontinuities, as in a customary finite element analysis.

[28] Sampling will therefore be carried out, not over the entire field, but one field partition at a time. In effect, this solves the problem of sampling an entire two-dimensional field by distributing the field over multiple partitions, and considering each partition as a unique sampled variable.

[29] In order to partition a mesh into equal-area surfaces, each of which must have at least one node, partitioning algorithms are used, based on the CHACO Software for Partitioning Graphs [*Hendrickson and Leland*, 1995]. This partitioner was initially designed with the goal of reducing parallel computing time for matrix solutions in finite element analysis or other computational areas. It allows for a wide variety of parallel machine architectures, and performs partitioning based on a nodal graph of the finite element connectivity, as well as geometrical information. Specifically, CHACO relies on the coordinates of the nodes to split meshes into equal area partitions. It has three primary global partitioning methods: Kernighan-Lin (K-L), inertial, and spectral, all of which can be used recursively. In order to facilitate a seamless integration of its partitioning routines into ISSM, CHACO was reworked and integrated as a module (see Figure 2). This ensures that partitioning is entirely consistent with the ISSM generated meshes, and fed to the DAKOTA software though the ISSM I/O routines.

[30] In our study, we use CHACO's inertial method, which produces the most regularly shaped partitions, in the shortest amount of time. In order to take into account the size of the elements, which CHACO relies on, each element area of the anisotropic mesh is divided by its number of nodes, and that area is assigned to the weighting of each node for partitioning. CHACO then computes the principal mesh axis using the nodal locations and weights, and then divides the structure into equal parts by planes orthogonal to the principal axis. One, three, or seven planes, denoted by bisection, quadrisection, or octasection, respectively, may be used. This leads to a banded appearance for the global partitioning, but when coupled with the Kernighan-Lin local optimization, this can be significantly improved. The process is recursive depending on the number of partitions requested.

[31] The effect of the weighting can be shown with respect to a reduced size anisotropic mesh of PIG. In Figures 3a–3c, the mesh is partitioned without equal-area weighting. As a result, the partitions, shown in red, vary widely in area, and the accompanying histograms show that while the partitions each have nearly the same number of nodes, the areas vary by 30% from smallest to largest. In contrast, in Figures 3d–3f, the mesh is partitioned with equal-area weighting. Consequently the partitions (in red) look visually similar, and the accompanying histograms show that the partitions have a number of nodes that also varies by almost 30% while the areas are approximately the same.

3. Validation

[32] ISSM, DAKOTA and CHACO are all thoroughly verified (ensuring that the equations in the software are correctly solved for) and validated (ensuring that the model accurately reproduces observations of processes it is designed to capture).

[33] To extend this level of confidence to the new capability, we carry out two sets of tests (presented in Table 2) based on a synthetic square ice sheet/ice shelf (1000 km $\times$ 1000 km) of thickness 1000 m at the ice divide, decreasing constantly to 300 m at the ice front. Ice flow is constrained on three sides, with an ice front on the fourth side. Ice becomes afloat 500 km downstream of the ice divide. Mass flux is computed through a 600 km across-flow fluxgate at the grounding line. Sampling is carried out on the ice thickness, assuming a relative standard deviation σ of 1%. The test mesh comprises 68 elements and 44 vertices, which is small enough that a large number of samples can be considered in the test. With this mesh, a maximum number of partitions of 44 can be chosen, which corresponds to the number of vertices in the mesh.

[34] Two tests are carried out, one where the number of partitions is kept constant and equal to 20 and the number of samples is increased from 2 to 1000; and another one where the number of samples per partition is kept constant and equal to 20 and the number of partitions is increased from

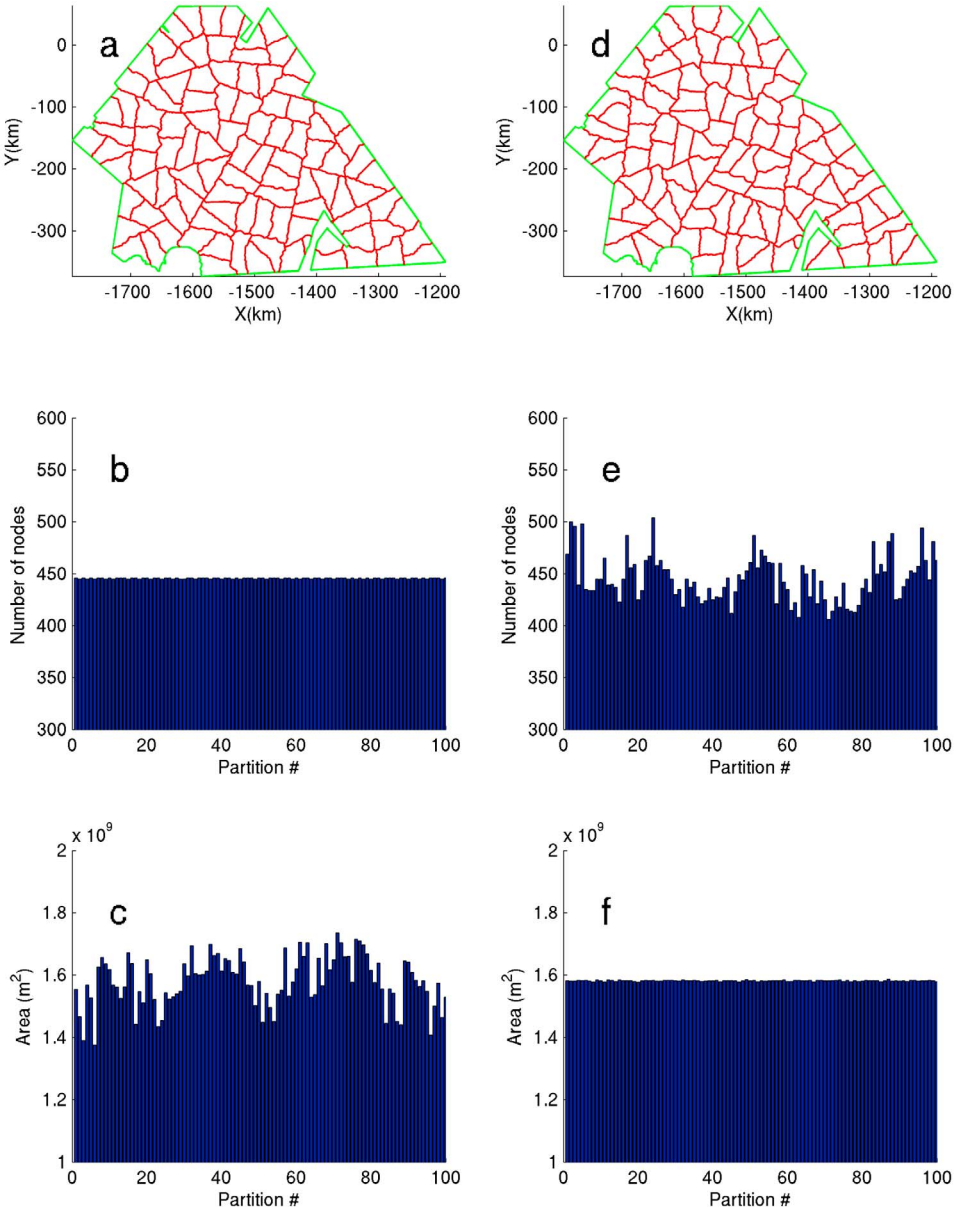

Figure 3. (a) Partitioning (in red) of PIG mesh into 100 partitions using CHACO and a non-weighted algorithm. (b) Number of nodes in each partition. (c) Total area weight of each partition (d, e, and f). Ditto using a weighted algorithm.

2 to 44. For both tests, we compute the mass flux average and standard deviation in Gt/yr at the grounding line. The first test shows how our Monte-Carlo simulation converges to constant averages and standard deviations between 200 to 500 samples, i.e. between 10 to 25 samples per partition. The second test demonstrates strong convergence of the Monte-Carlo simulation when the number of partitions is increased toward its maximum, which is the number of vertices in the mesh.

[35] A final test is also carried out to analytically verify our new capability. We use ISSM in stand-alone mode to compute importance factors for mass fluxes, using hand derived input parameter distributions. With this test, we can verify and validate the computations of statistics by DAKOTA, and the correct implementation of I/O between ISSM and DAKOTA.

4. Data and Model Setup

[36] InSAR surface velocities are available for the PIG area from *Rignot* [2008]. These velocities were processed for the year 1996, and coverage is extensive and of good quality, making inversion of unknown parameters such as the basal drag coefficient reliable [*Morlighem et al.*, 2010]. Thicknesses are also available extensively, thanks to the 2004/05 AGASEA/BBAS survey [*Holt et al.*, 2006; *Vaughan et al.*, 2006] and the 2009 Operation IceBridge campaign [*Allen*, 2009]. Model setup is therefore possible

Table 1. Data Sets Used for the PIG Model Setup[a]

Field	Data Set Origin
Surface Velocity and Grounding Lines	*Rignot* [2008]
Thickness, Surface and Bed	*Holt et al.* [2006], *Vaughan et al.* [2006], *Allen* [2009]
Geothermal Flux	*Shapiro and Ritzwoller* [2004]
Surface Temperatures	*Ettema et al.* [2009]

[a]First column shows the field of interest. Second column shows the origin of data set.

for the entire PIG basin. Other data sets used to initialize the ice flow model, which can be found summarized in Table 1, include the geothermal heat flux from *Shapiro and Ritzwoller* [2004] and surface temperatures from *Ettema et al.* [2009]. These data sets are used to carry out a steady state thermal model of PIG, which is used to compute the ice hardness B. An inversion for the basal drag coefficient α is then carried out, for which the temperature is kept constant. H, B and α are shown in Figures 4a, 4c, and 4d. These three model results are then used as input parameters for sampling and local reliability analyses. The anisotropic mesh used for the study comprises 89,000 elements, with resolutions ranging from 3 km in the interior of the basin, to 1km at the shear margins and near the grounding line.

[37] For ice thickness, Ground Penetrating Radar (GPR) cross-over errors measurements are available from the 2009 Operation IceBridge campaign, and are provided by the Center for Remote Sensing of Ice Sheet (CReSIS). These cross-over errors do not cover the entire PIG basin, but they are the only reliable estimate of thickness measurement errors available in the area. We extrapolate them wherever CReSIS thickness measurements are missing, and where AGASEA thicknesses are used. The resulting error distribution is shown in Figure 4b. The cross-over errors are also filtered to discard extreme values in locations where thicknesses are very small, and for which ice flow is essentially stagnant, such as in mountainous areas. These cross-over errors are then used to calibrate the 3σ value for a normal distribution of the thickness parameter, and the diameter for a uniform distribution of the thickness parameter. Examples of the statistical distributions of ice thickness are shown in Figure 5 for locations adjacent to fluxgates 2, 3 and 4 respectively. Similar statistical distributions are used for each partition of the mesh. Not knowing the statistical type of distribution for thickness, we choose to run two sampling analyses, one with a normal distribution, another one with a uniform distribution. Two thousand sample runs are carried out for both types of distributions, using 100 partitions. This is equivalent to approximately 20 samples per partition. As seen in Figure 5, this number of samples is statistically significant, as it is capable of capturing the tails of the normal and uniform distributions. It also corresponds to the number of samples per partitions for which our verification model

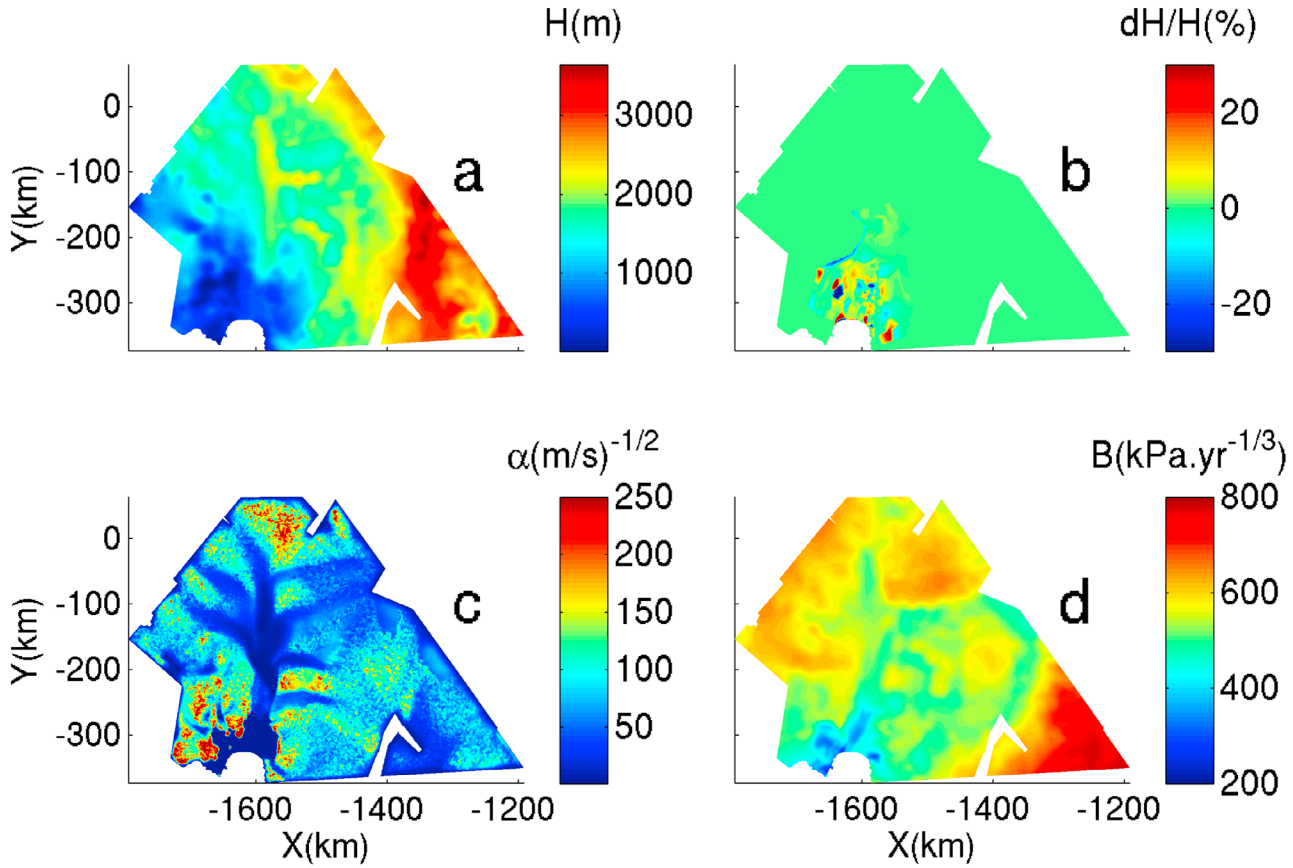

Figure 4. Parameter inputs for ice flow model on PIG: (a) thickness H in m, (b) cross over errors (in %) from CReSIS center, (c) inverted basal drag coefficient α in $(m/s)^{-1/2}$ and (d) depth-averaged ice hardness B in $kPa.yr^{-1/3}$.

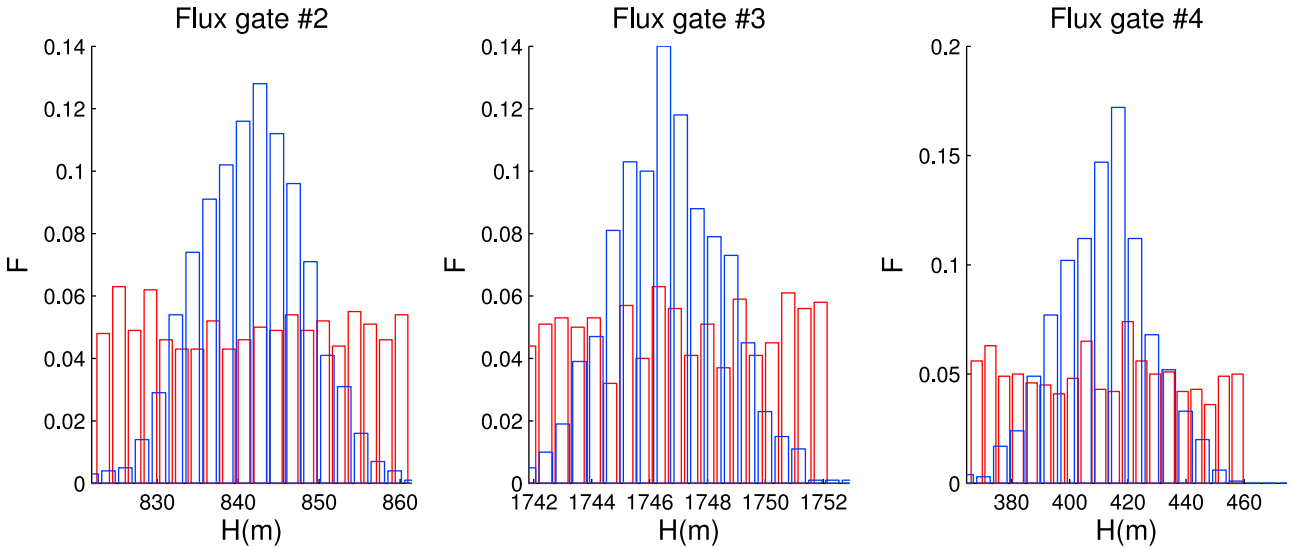

Figure 5. Thickness histograms for uniform (red) and normal (blue) statistical distributions near fluxgates 2, 3 and 4 (see Figure 1). All three distributions were calibrated using the thickness data sets from Operation IceBridge [*Allen*, 2009] and corresponding cross-over errors. For normal distributions, the 3σ deviation was taken equal to half the cross-over errors. For uniform distributions, the diameter was taken equal to the cross-over errors. The x-axis of each histogram represents ice thickness H in m and the y-axis represents the frequency F (between 0 and 1). Each histogram contains 2000 samples for 20 bins of 100 samples each.

converges (Table 2). The runs are carried out on the NASA Advanced Supercomputing (NAS) Pleiades cluster, using Westmere type Intel CPUS (160 cpus), each run taking approximately 2 hours to complete. In addition, given the performance of the runs, we are able to analyze the impact of increased noise in the observations, by augmenting the standard deviation 3, 5, 7 and 10 times respectively, and running the corresponding sampling analyses.

[38] Finally, we carry out a local reliability analysis of PIG, using as model inputs, ice thickness H, basal drag coefficient α and ice hardness B. Normal distributions are specified for all three parameters, using standard deviations of 5 %. The goal is to evaluate the sensitivity of mass outflux at the thirteen gates described in Figure 1, with respect to all three model inputs. Choosing identical standard deviations also ensures that we can carry out meaningful input-to-input comparisons, and conclude on which parameter mass flux is most sensitive to.

5. Results

[39] Results of sampling and local reliability studies on PIG are shown in Figures 6, 7, 8 and 9. Figure 6 shows the statistical distribution of mass flux through each gate, carried out for sampling of the thickness using a uniform (in red) and normal statistical distribution (in blue) respectively. Mass flux average μ and standard deviation σ are also provided for each distribution. Both μ and σ are computed by fitting normal distributions to the output results. This fit is good for most fluxgates, with the notable exception of gate 10, for which mass flux is clearly uniformly distributed in the case of a uniform perturbation in ice thickness. The thirteen gates used for mass flux computations are distributed along the tributaries, as shown in Figure 1. For each one of these gates, average mass flux ranges from 2.8 Gt/yr for the smallest upstream tributaries to 66 Gt/yr along the main glacier. As expected, these values are identical irrespective of the type of noise specified for the input thickness. They also provide independent validation of our new sampling capability. The standard deviations for each fluxgate ranges from 5.2_e–4% to 3.3% (here, % is with respect to the input average μ) for a uniform distribution of the ice thickness, and from 3.2_e–4% to 1.8% for a normal

Table 2. Verification of Sampling Capabilities for the ISSM-DAKOTA Integrated Model[a]

Number of Samples	μ (Gt/yr)	σ (Gt/yr)	Number of Partitions	μ (Gt/yr)	σ (Gt/yr)
2	398.3	8.410	2	395.1	5.070
5	395.4	3.297	5	395.1	4.701
10	395.0	4.543	10	395.1	3.901
20	395.1	3.097	20	395.1	3.542
50	395.1	3.505	44	395.1	3.476
100	395.1	3.568			
200	395.1	3.502			
500	395.1	3.521			
1000	395.1	3.525			

[a]This test is for a square synthetic ice sheet/ice shelf system, (1000 km × 1000 km) of thickness 1000 m at the ice divide, decreasing constantly to 300 m at the ice front (see text for more details). Mass flux averages μ and standard deviations σ are computed first for sampling analyses with increasing number of samples per partition (first, second and third column) and second for sampling analyses with increasing number of partitions at equal number of overall samples (fourth, fifth and sixth columns). Averages and standard deviations are in Gt/yr, computed at the grounding line of the ice sheet/ice shelf system.

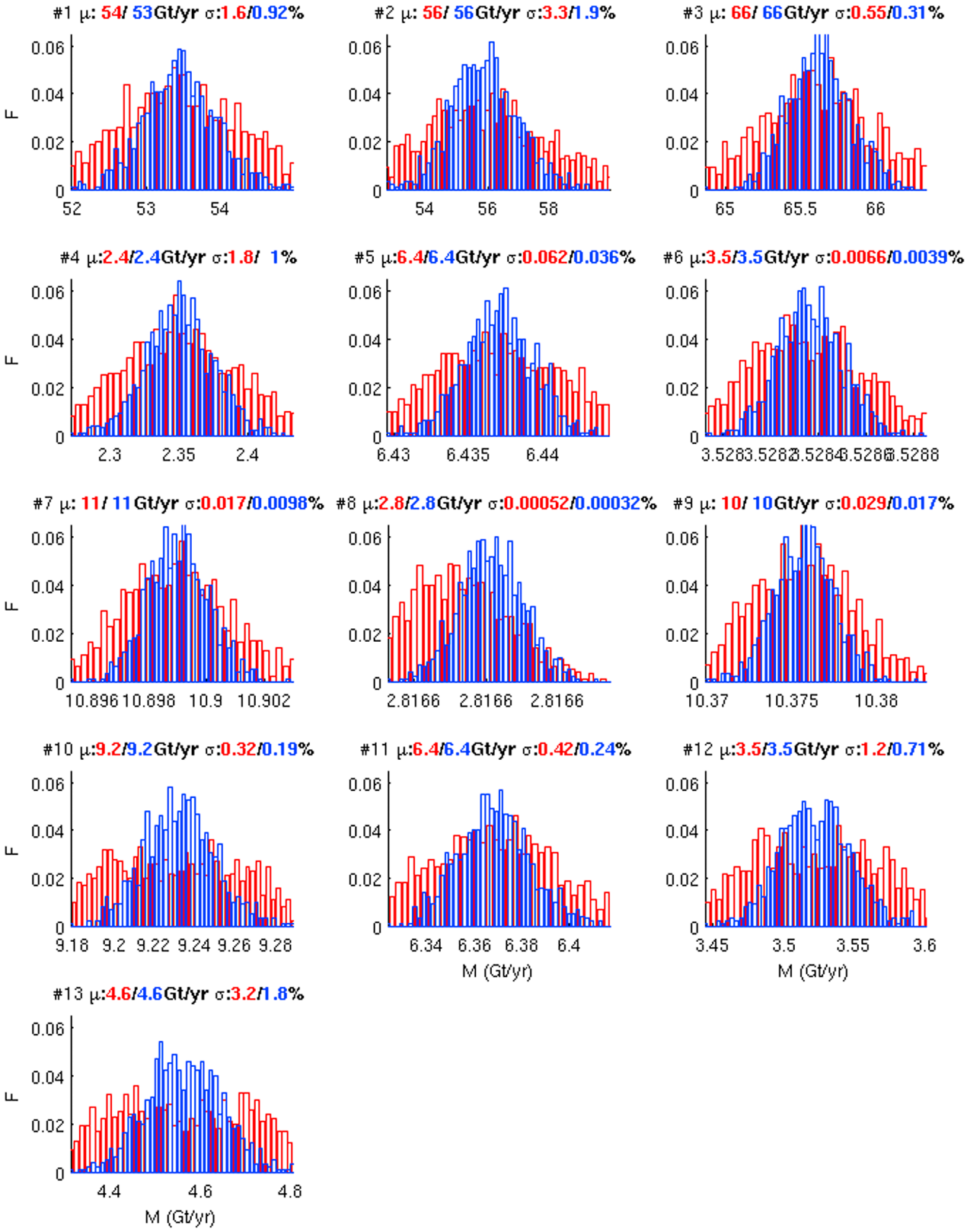

Figure 6. Histograms for mass flux computations across gates specified in Figure 1. For these runs, ice thickness is sampled using a normal distribution (blue color) and a uniform distribution (red color). For the normal distribution, the 3σ deviation is taken equal to half the thickness cross-over errors. For the uniform distribution, the radius is taken equal to half the cross-over errors. Mean and standard deviations are supplied for each gate and for each type of distribution. Mass fluxes M are expressed in Gt/yr and frequencies F are between 0 and 1.

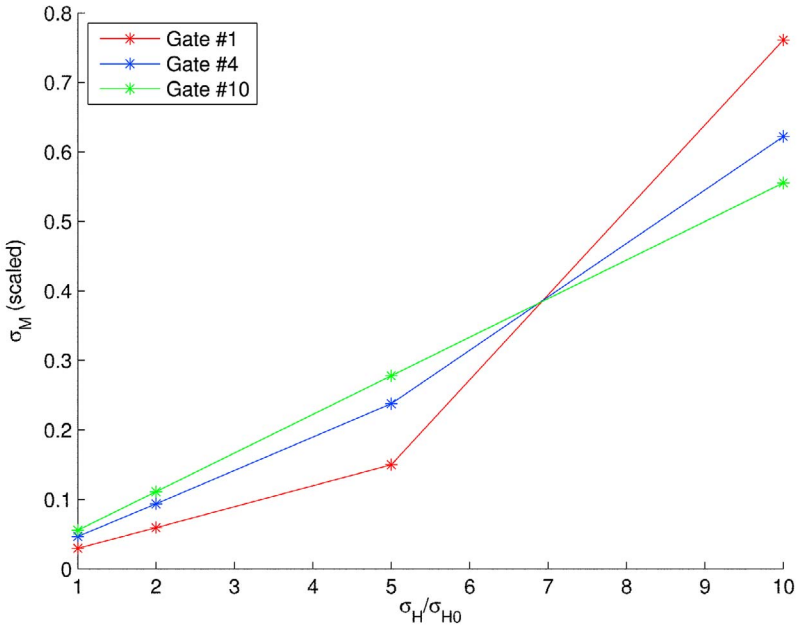

Figure 7. Evolution of mass flux standard deviation σ_M when thickness error margins are increased from an initial standard deviation σ_{H0} to a larger standard deviation σ_H, for fluxgates 1, 4 and 10 (see Figure 1). Each σ_M has been scaled, so as to make the comparison between fluxgates easier. Fluxgates 1, 4 and 10 are representative of the trends in variations observed for all other gates.

distribution of the ice thickness. For a given fluxgate, the standard deviation corresponding to a uniform thickness distribution is on average twice the standard deviation corresponding to a normal distribution. This is also observed in the shape of the mass flux tails. For a uniform thickness distribution, these tails are more elongated, which implies that extreme values are not filtered out as much.

[40] Overall, the response of the SSA ice flow model to input errors is surprisingly smooth. For almost all fluxgates, the mass flux distribution is normal in nature, with standard deviations on the order of 2%. This result indicates that regardless of the noise level in the thickness, the mass flux response over the entire basin clusters around the ice flow average behavior. Of course, the nature of the noise (uniform vs normal) introduces differences in the system response, but not to the extent that one would have expected. Indeed, the ice flow model acts as a filter in which extreme responses to input noise are smoothed out.

[41] Figure 7 shows how the mass flux standard deviation scales when the thickness standard deviation is increased uniformly across the entire basin. As observed, the standard deviation scales linearly for most fluxgates. Even when the noise level reaches 100% of the input thickness, the model still responds in a linear manner. The only exception is found at the ice front (gate 1) , where we suspect the number of samples is not sufficient. The result is a mass flux distribution for which the average μ is significantly different for high values of the input standard deviation.

[42] Figure 8 shows local reliability results for the mass flux advecting through the 1996 PIG grounding line. The same results are displayed in Figure 9 for fluxgate 10. Importance factors are computed for ice thickness H (Figure 8a), basal drag coefficient α (Figure 8b), and ice hardness B (Figure 8c). Ratios of importance factors are computed for ice thickness to basal drag coefficient (Figure 8d), ice thickness to ice hardness (Figure 8e), and basal drag coefficient to ice hardness (Figure 8f). All results are displayed using a logarithmic scale. For each parameter, the importance factor represents how sensitive the mass flux is to local variations in the input parameter. As expected, mass flux is significantly sensitive to each input parameter. This sensitivity decreases exponentially with distance to the fluxgate, and is channeled along flowlines, upstream and downstream of the fluxgate. At a distance of 100 km from the fluxgate, upstream or downstream, sensitivity decreases by almost 3 orders of magnitude. This result quantifies exactly how far sensitivity to input parameters noise reaches out, and how diffuse this area of influence is around the fluxgate being considered.

[43] Differences between sensitivities to H, α and B are important. The parameter to which mass flux is most sensitive is ice thickness, followed equally by α and B. Sensitivity to α naturally goes to zero at the ice shelf, which is expected given that basal friction under an ice shelf is equal to zero. The extent to which mass flux is sensitive to thickness is large indeed, going upstream almost 250 km. The sensitivity to α and B does not extend as much. This is a significant difference between all three input parameters, which was not obvious given the seemingly equal roles H, α and B play in the equations of ice flow for the SSA model. Ratios of importance factors further confirm this conclusion: mass flux is at least 100 times more sensitive to ice thickness than to basal drag coefficient or ice hardness. For distances larger than 50 km from the fluxgate, this ratio increases to 1000. The only exception to this result is found on the PIG ice shelf, for which mass flux is equally sensitive to ice hardness and thickness (Figures 8e and 9e), and not sensitive at all to the basal drag coefficient, as explained above.

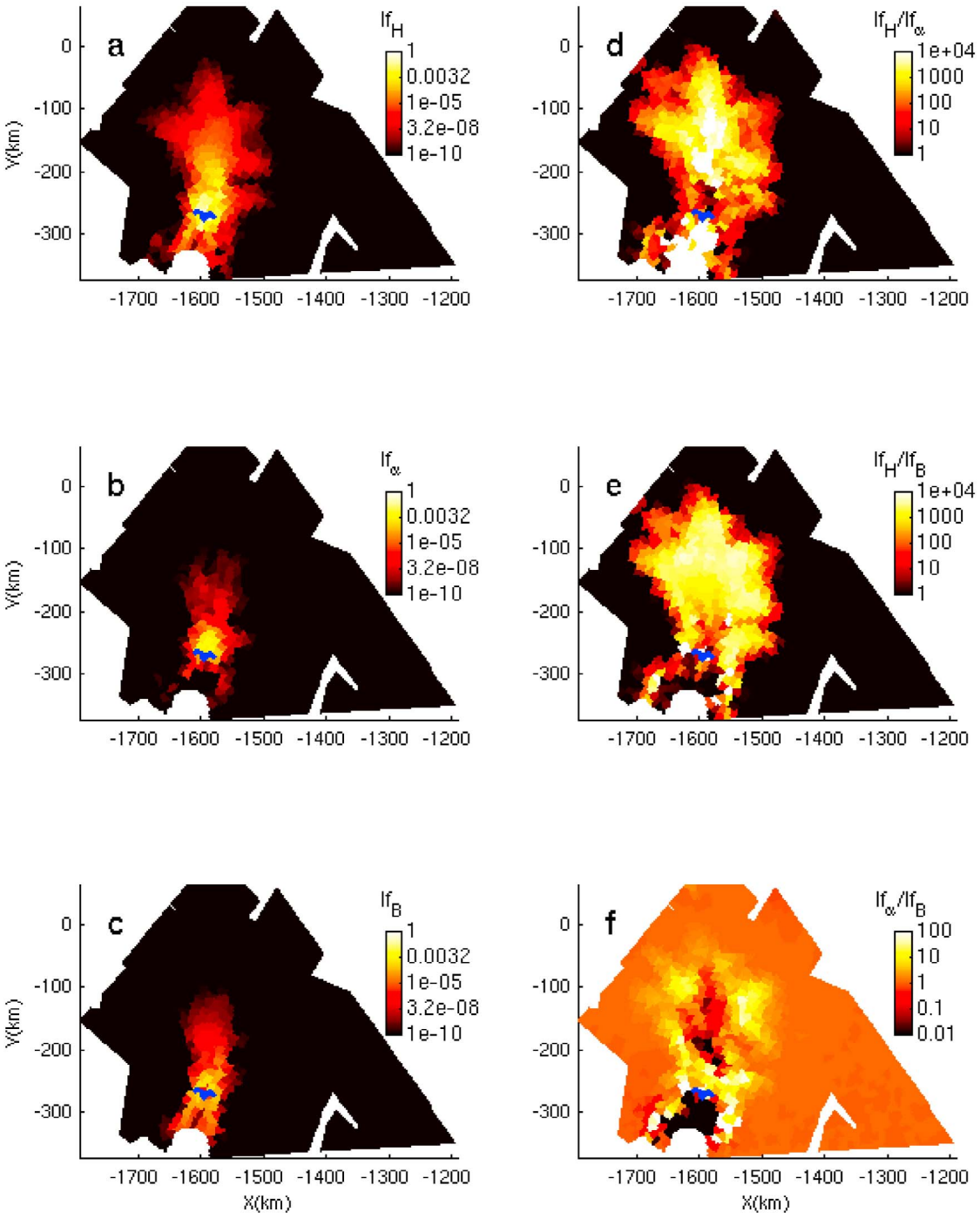

Figure 8. Importance factors (from equation (7)) for the mass outflux at the 1996 grounding line (gate 2 in Figure 1, outlined in blue on all frames), for (a) thickness, (b) basal drag coefficient and (c) ice rigidity. (d) Ratio of thickness to basal drag coefficient importance factor. (e) Ratio of thickness to ice hardness importance factor. (f) Ratio of basal drag coefficient to ice hardness importance factor.

[44] Figure 9 is interesting in that it shows how mass flux sensitivity for a tributary of the main glacier extends over several tributaries. From gate 10, mass flux sensitivity to variations in input parameters reaches gates 5, 6, 7 and 8. This is a surprising result that tends to show how one tributary is strongly coupled to the flow of its surrounding tributaries. This is especially the case for sensitivity to variations in thickness, which reaches far upstream of neighboring tributaries, almost 200 km away.

6. Discussion

[45] The results presented here are surprising in several ways, with important implications for improving projections

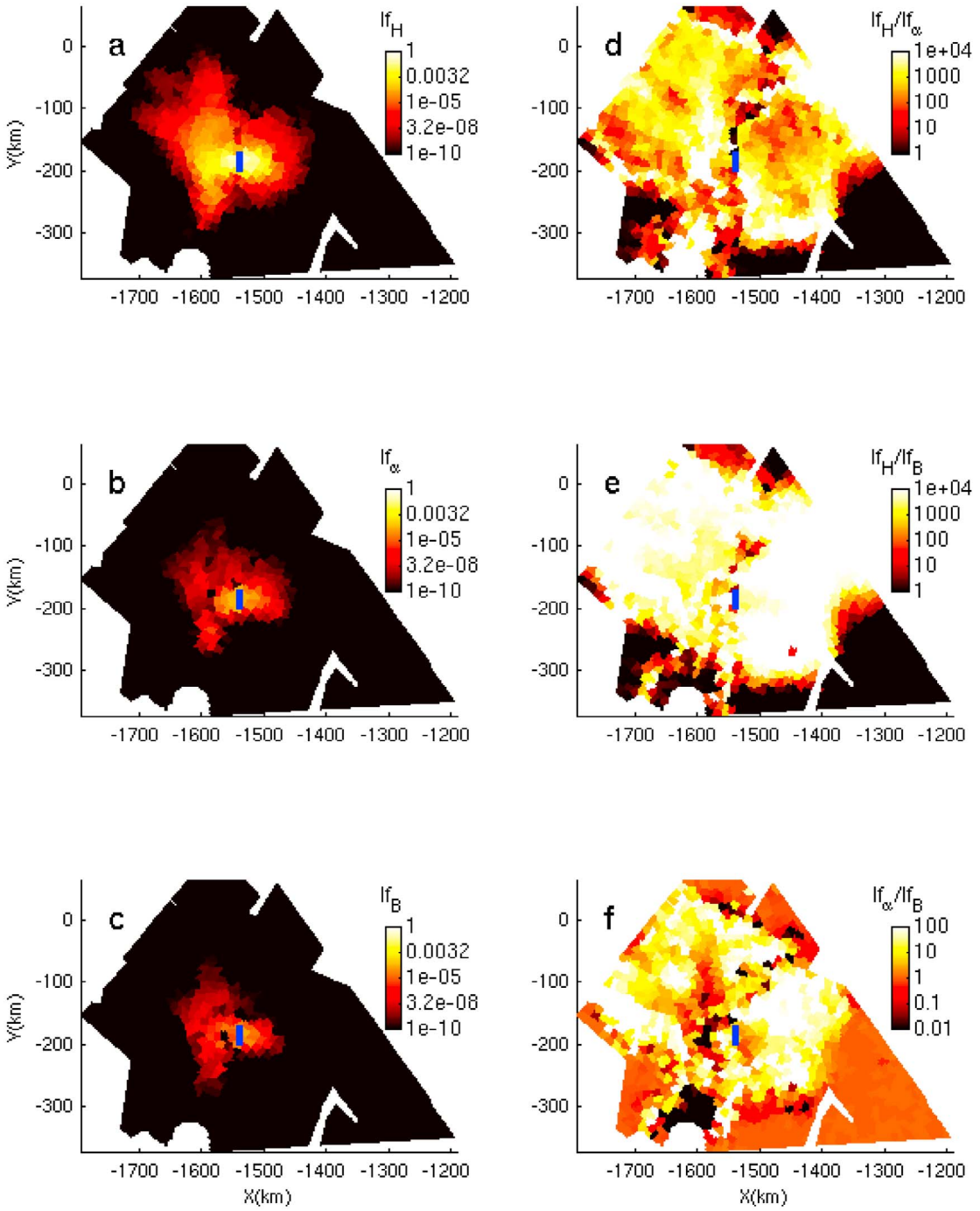

Figure 9. Importance factors (from equation (7)) for the mass outflux at gate 10 in Figure 1 (outlined in blue on all frames) for (a) thickness, (b) basal drag coefficient and (c) ice rigidity. (d) Ratio of thickness to basal drag coefficient importance factor. (e) Ratio of thickness to ice hardness importance factor. (f) Ratio of basal drag coefficient to ice hardness importance factor.

of future mass balance for PIG, and for ice streams across Antarctica in general.

[46] First, the SSA model is stable with respect to errors in the ice thickness and their impact on mass fluxes. This conclusion holds irrespective of the nature of the noise (normal or uniform) or location of the fluxgate. The mass flux histograms cluster around an average mass flux determined by the average modeled ice flow, with distribution tails that are consistently small. The stability of the SSA model with respect to uncertainties in ice thickness is such that diagnostic studies of the mass balance of PIG are possible, even given the large uncertainties in thickness data sets. This conclusion is surprising in that a more non-linear response would have been expected, given the highly non-linear behavior of ice [*Glen*, 1955]. However, the reason the SSA model behaves as it does probably lies in the fact that it

is linearly dependent on ice thickness because it vertically averages the stress equilibrium equations. This will tend to average responses to input variations in thickness. However, this result could also indicate that SSA is not a valid model for application to the entire Pine Island Glacier, and that the assumption of plug-flow made here is the issue. To answer this question, we computed the magnitude of the deflection (in m/yr) between the bed and the surface for a full-Stokes model, based on the results from *Morlighem et al.* [2010]. For all our fluxgates, the deflection was less than 1% of the overall depth-averaged velocity, except for fluxgates 10 and 11, where it reached from 1% to 5% of the depth-averaged velocity. This means that for PIG, the SSA model misses less than 1% of the mass flux at almost all the flux gates, even the ones positioned far inland in the tributaries. This effectively demonstrates that our results are not an artifact of the SSA model, and that the conclusions presented here are robust. For fluxgates 10 and 11, and for locations more inland, the SSA model should probably be improved upon, either using a full-Stokes model [*Morlighem et al.*, 2010] or, if computational considerations are important such as here for sampling analyses, using a hybrid model such as the [*Pollard and DeConto*, 2009; *Hindmarsh*, 2004]. Another aspect that could somewhat impact our conclusions is the lack of transient representation in the thermal model used to initialize B, due to the intense computational requirements of basal inversions. As suggested by *Larour et al.* [2012], the type of temperature offset to observations incurred by this approach is at least 2°C for an ice sheet such as the Greenland Ice Sheet. A simple forward run of the PIG model shows that such a temperature differential would result in an increase in depth-averaged velocity (and therefore in mass flux) of 6 to 9%. This is significant compared to the errors presented in Figure 6, and shows that further study is required if conclusions of our study are to be extended to transient ice flow models.

[47] Our scalability study shown in Figure 7 confirms our findings for steady state regimes of ice flow, and demonstrates a linear response of the model to a linear increase in the error margins specified for the input thickness. Further studies are required to extend this conclusion to higher-order models such as the Blatter/Pattyn model (BP) [*Blatter*, 1995; *Pattyn*, 1996], or the full-Stokes model (FS) [*Stokes*, 1845], especially given the sensitivity of the latter to vertical bridging effects near the grounding line [*Morlighem et al.*, 2010]. Another issue that will arise in transient models is the coupling between the stress-equilibrium and mass conservation equations [*Larour et al.*, 2012]. Mass conservation is not included in the model at all, and this new component will impact mass fluxes heavily. In particular, the grounding line area will need to be correctly retreated or advanced [*Schoof*, 2007b, 2007b; *Durand et al.*, 2009; *Nowicki and Wingham*, 2008], as there is a strong link between the mass flux and the ice thickness in this area. Indeed, we believe our results will be significantly different in the lower parts of the ice sheet, where dynamic ice flow acceleration from ungrounding of the ice stream are most susceptible to be the driver of mass flux changes. Similarly, another conclusion of our analysis is that error analyses of simple ice flow models such as 2D SSA can probably be carried out using simpler surrogate models. Indeed, as shown by our scaling analysis in Figure 7, the diagnostic response to increased errors in model inputs scales linearly. This result is significant in that it allows for a rapid assessment of the error propagated from inputs to diagnostics, without relying on expensive sampling analyses.

[48] Indeed, we show here that the SSA model tends to dampen strong perturbations in the system. The same type of conclusions was reached for applications of control methods to the inversion of basal friction in the Ross Ice Shelf ice streams [*MacAyeal*, 1989, 1992]. In this type of studies, it was shown that noise in surface velocity observations does not perturb inversion results for the basal friction. Similarly, our sampling analysis demonstrates that the range of error margins in modeled mass flux is less than 3%, despite error margins specified for the input thickness parameter ranging from −30 to +30% (Figure 4b). Furthermore, these results appear to remain valid near the grounding line, where the largest errors in the CReSIS thickness data set are concentrated and despite the fact that this area is one of the most sensitive to changes in the ice thickness, as demonstrated by *Schoof* [2007a, 2007b], *Nowicki and Wingham* [2008] and *Durand et al.* [2009] in this type of study. Our model does not include grounding line dynamics, but it still takes the hydrostatic equilibrium of the ice shelf into account, and one would therefore expect larger error ranges. Our results seem to indicate that in forward mode, such errors in ice thickness do not significantly affect mass flux at the grounding line. The hope is that such results would extend to transient ice flow simulations. If it is the case, then current thickness observations would prove sufficient to project the mass balance of PIG in the near future. Further sampling studies in prognostic mode are therefore required.

[49] Second, we demonstrate that thickness is the most important parameter to specify when relying on the SSA ice flow model for capturing the mass balance of PIG. Our results show that mass flux is most sensitive to errors in the thickness parameter. This sensitivity extends over a large spatial area, which reaches far upstream and downstream of each considered fluxgate. The model is of course also sensitive to variations in local basal friction and ice hardness, but to a lesser extent. The only exception, as remarked in the results, is on the PIG ice shelf, where mass flux is equally sensitive to ice hardness and ice thickness, and not sensitive to basal friction. When looking at the ice flow equations of the SSA model [*MacAyeal*, 1989], this conclusion is not so obvious given the strong non-linearity present in the ice rheology (cubic dependence of viscosity on stress) and basal friction law. Of course, this conclusion is reached while assuming equally distributed errors in the input parameters H, α and B (5% standard deviation), and normal statistical distributions. This assumption came from our lack of knowledge of the type of errors that influences ice hardness and basal friction, and from the need to compare sensitivities between parameters with equivalent error margins. A thorough analysis of the error margins affecting B and α are outside the scope of the present study, but this preliminary analysis is in line with current understanding of what parameterizations of an ice sheet model are most critical [*Joughin et al.*, 2010; *Seroussi et al.*, 2011].

[50] The implications for ongoing and future data collection campaigns such as Operation IceBridge, IceSat-2 or Cryosat-2 among others are important. Our results can be used to quantify the impact of current data measurements on

the quality of ice flow models, especially with respect to the thickness of the ice sheet, or equivalently, the bedrock position. They indicate that for equivalent error margins, thickness is the most important parameter to measure. On ice shelves, this conclusion is less certain, and the thermal regime of the ice shelf, as well as the ice fabrics [*Paterson*, 1994] could play an important role in controlling ice flow. These results also have to be tempered by the fact that comprehensive knowledge of the uncertainties in the specification of ice hardness as well as basal friction is currently unavailable. If we were to assume larger error margins for ice hardness, which is probably in order given the large uncertainties in the specification of the geothermal flux [*Shapiro and Ritzwoller*, 2004], our results could be significantly different. In addition, ice thickness errors are only specified at the locations were cross-over errors are available. This does not preclude such errors being much larger on flight tracks located between cross-overs. Presently, there does not exist a comprehensive error propagation model for the IceBridge data set used in this study, which makes it impossible to assess the validity of cross-over errors as a proxy for the rest of the glacier. However, it is to be noted that the shape of the ice sheet/ice shelf is not free of physical constraints, and that mass conservation acts as a strong bound on the shape of the glacier [*Morlighem et al.*, 2011], so that wide variations between cross-over locations is not likely to occur. Further study is definitely required to understand whether mass conservation could be used in conjunction with cross-overs to build an error model of ice thickness over the whole of PIG, for use in uncertainty quantification of ice flow models.

[51] Another implication stemming from our results is that modeling the mass flux of a certain gate cannot be done using a flowline approach, in which thickness is measured upstream and downstream of the gate only. Neighboring tributaries are very influential in the mass flux evolution of a local gate. A mechanism of entrainment seems most probable to explain this effect, where variations in ice flow from a neighboring tributary impacts ice flow downstream of the fluxgate, which then increases driving stress locally, hence modifying ice flow at the fluxgate. This type of effect was used to try and explain the propagation of kinematic waves upstream of a glacier, following major perturbation events such as calving of an ice front, or collapse of an ice shelf [*Payne et al.*, 2004; *Howat et al.*, 2007]. This again has implications for data collection campaigns, as it tends to show that model improvements for the mass balance of an ice stream cannot be reached by targeting specific flow lines only. Spatial coverage of thickness measurements needs to be extensive, reaching areas that extend hundreds of kilometers from the point of interest. More specifically, if we take Figures 8 and 9 and a threshold of $If = 0.001$ (*If* the importance factor) to quantify the extent of the area where mass flux is sensitive to model inputs, we measure an area of 150 km around the fluxgate for ice thickness H, 50 km for the basal drag coefficient α and 30 km for ice hardness B.

7. Conclusions

[52] We present a new integrated model that merges ice flow modeling capabilities from ISSM with sampling and local reliability methods from DAKOTA. This new capability helps quantify the sensitivity of ice flow models to input parameters such as thickness, basal friction or ice hardness. We apply this new approach to the Pine Island Glacier, for which we demonstrate that, given equal error margins in the input data sets (ice thickness, ice hardness and basal friction at the ice/bed interface), ice thickness is the most critical model input for modeling mass balance. We show that the SSA model, which is widely used to model fast flowing ice streams, acts as a filter to dampen noise found in thickness observations. This filter scales linearly with the magnitude of the noise in the input parameters. We also show that in order to model mass flux efficiently, a large extent must be considered in the specification of model inputs, and that a flowline approach cannot capture such extent efficiently. Our results are directly applicable to airborne data collection campaigns, for which scientific requirements are difficult to establish because they tend to rely on the knowledge we have of underlying processes controlling ice flow and the mass balance of glaciers. Our results also seem to suggest that current error margins in data collected by airborne campaigns may be sufficiently precise for short-term projections of mass balance in large ice streams of Antarctica or Greenland. We also demonstrate the need to further quantify the increase in uncertainties due to dynamic effects in transient models (especially near the grounding line) and to improve the specification of model inputs such as ice hardness and basal friction, which cannot be measured but only modeled.

[53] **Acknowledgments.** This work was performed at the Jet Propulsion Laboratory, California Institute of Technology, at the Department of Earth System Science, University of California Irvine, and at Laboratoire MSSMat, École Centrale Paris, under a contract with the National Aeronautics and Space Administration, Cryospheric Sciences Program and Modeling Analysis and Prediction Program, and a contract with the Jet Propulsion Laboratory Research Technology and Development Program. Resources supporting this work were provided by the NASA High-End Computing (HEC) Program through the NASA Advanced Supercomputing (NAS) Division at Ames Research Center. The authors would like to acknowledge Operation IceBridge data used in the study, as well as CReSIS data generated from NSF grant ANT-0424589 and NASA grant NNX10AT68G. They would also like to thank P. Heimbach and J. Johnson for their insightful comments during the review.

References

Allen, C., (2009), IceBridge MCoRDS L2 Ice Thickness, http://nsidc.org/data/irmcr2.html, Natl. Snow and Ice Data Cent., Boulder, Colo.

Blatter, H. (1995), Velocity and stress-fields in grounded glaciers: A simple algorithm for including deviatoric stress gradients, *J. Glaciol.*, *41*, 333–344.

Brinkerhoff, D., T. Meierbachtol, J. Johnson, and J. Harper (2011), Sensitivity of the frozen-melted basal boundary to perturbations of basal traction and geothermal heat flux: Isunnguata Sermia, western Greenland, *Ann. Glaciol.*, *52*, 43–50.

Coleman, H. W., and W. G. Steele Jr. (1989), *Experimentation and Uncertainty Analysis for Engineers*, John Wiley, New York.

Durand, G., O. Gagliardini, T. Zwinger, E. Le Meur, and R. Hindmarsh (2009), Full Stokes modeling of marine ice sheets: Influence of the grid size, *Ann. Glaciol.*, *50*, 109–114.

Eldred, M. S., et al. (2008), DAKOTA, a multilevel parallel object-oriented framework for design optimization, parameter estimation, uncertainty quantification, and sensitivity analysis, Version 4.2 User's Manual, *Tech. Rep. SAND2006-6337*, Sandia Natl. Lab., Albuquerque, New Mexico.

Ettema, J., M. R. van den Broeke, E. van Meijgaard, W. J. van de Berg, J. L. Bamber, J. E. Box, and R. C. Bales (2009), Higher surface mass balance of the Greenland Ice Sheet revealed by high-resolution climate modeling, *Geophys. Res. Lett.*, *36*, L12501, doi:10.1029/2009GL038110.

Giering, R., and T. Kaminski (1998), Recipes for adjoint code construction, *ACM Trans. Math. Software*, *24*, 437–474.

Glen, J. (1955), The creep of polycrystalline ice, *Proc. R. Soc. A*, *228*, 519–538.

Greve, R. (1997a), A continuum-mechanical formulation for shallow polythermal ice sheets, *Phil. Trans R. Soc. A*, *355*, 921–974.
Greve, R. (1997b), Application of a polythermal three-dimensional ice sheet model to the Greenland Ice Sheet: Response to steady-state and transient climate scenarios, *J. Clim.*, *10*, 901–918.
Haldar, A., and S. Mahadevan (2000), *Probability, Reliability, and Statistical Methods in Engineering Design*, John Wiley, New York.
Hascoët, L. (2004), Tapenade: A tool for automatic differentiation of programs, paper presented at 4th European Congress on Computational Methods, ECCOMAS'2004, Dep. of Math. Inf. Tech., Univ. of Jyvaskyla, Jyvaskyla, Finland.
Heimbach, P., and V. Bugnion (2009), Greenland ice-sheet volume sensitivity to basal, surface and initial conditions derived from an adjoint model, *Ann. Glaciol.*, *50*, 67–80.
Hendrickson, B., and R. Leland (1995), The Chaco user's guide, version 2.0, *Tech. Rep. SAND-95-2344*, Sandia Natl. Lab., Albuquerque, New Mexico.
Hindmarsh, R. (2004), A numerical comparison of approximations to the Stokes equations used in ice sheet and glacier modeling, *J. Geophys. Res.*, *109*, F01012, doi:10.1029/2003JF000065.
Holt, J., D. Blankenship, D. Morse, D. Young, M. Peters, S. Kempf, T. Richter, D. Vaughan, and H. Corr (2006), New boundary conditions for the West Antarctic Ice Sheet: Subglacial topography of the Thwaites and Smith glacier catchments, *Geophys. Res. Lett.*, *33*, L09502, doi:10.1029/2005GL025561.
Howat, I. M., I. Joughin, and T. A. Scambos (2007), Rapid changes in ice discharge from greenland outlet glaciers, *Science*, *315*, 1559–1561.
Iman, R. L., J. C. Helton, and J. E. Campbell (1981), An approach to sensitivity analysis of computer models, Part 1. Introduction, input variable selection and preliminary variable assessment, *J. Qual. Tech.*, *13*, 174–183.
Joughin, I., D. MacAyeal, and S. Tulaczyk (2004), Basal shear stress of the Ross ice streams from control method inversions, *J. Geophys. Res.*, *109*, B09405, doi:10.1029/2003JB002960.
Joughin, I., J. L. Bamber, T. Scambos, S. Tulaczyk, M. Fahnestock, and D. R. MacAyeal (2006), Integrating satellite observations with modelling: basal shear stress of the Filcher-Ronne ice streams, Antarctica, *Phil. Trans R. Soc. A*, *364*, 1795–1814.
Joughin, I., B. Smith, I. Howat, T. Scambos, and T. Moon (2010), Greenland flow variability from ice-sheet-wide velocity mapping, *J. Glaciol.*, *56*, 416–430.
Khazendar, A., E. Rignot, and E. Larour (2007), Larsen B Ice Shelf rheology preceding its disintegration inferred by a control method, *Geophys. Res. Lett.*, *34*, L19503, doi:10.1029/2007GL030980.
Khazendar, A., E. Rignot, and E. Larour (2009), Roles of marine ice, rheology, and fracture in the flow and stability of the Brunt/Stancomb-Wills Ice Shelf, *J. Geophys. Res.*, *114*, F04007, doi:10.1029/2008JF001124.
Larour, E. (2005), Modélisation numérique du comportement des banquises flottantes, validée par imagerie satellitaire, PhD thesis, Ecole Centrale, Paris.
Larour, E., H. Seroussi, M. Morlighem, and E. Rignot (2012), Continental scale, high order, high spatial resolution, ice sheet modeling using the Ice Sheet System Model (ISSM), *J. Geophys. Res.*, *117*, F01022, doi:10.1029/2011JF002140.
MacAyeal, D. (1989), Large-scale ice flow over a viscous basal sediment: Theory and application to Ice Stream-B, Antarctica, *J. Geophys. Res.*, *94*, 4071–4087.
MacAyeal, D. (1992), The basal stress distribution of Ice Stream E, Antarctica, Inferred by Control Methods, *J. Geophys. Res.*, *97*, 595–603.
MacAyeal, D. (1993), Binge/Purge oscillations of the Laurentide ice-sheet as a cause of the North-Atlantics Heinrich events, *Paleoceanography*, *8*, 775–784.
McKay, M., R. Beckman, and W. Conover (1979), A comparison of three methods for selecting values of input variables in the analysis of output from a computer code, *Technometrics*, *21*, 239–245.
Metropolis, N., and S. Ulam (1949), The Monte Carlo method, *J. Amer. Stat. Associ.*, *44*, 335–341.
Morland, L. (1987), Unconfined ice shelf flow, paper presented at Workshop on the Dynamics of the West Antarctic Ice Sheet, Univ. Utrecht, Utrecht, Netherlands, May 1985.
Morlighem, M., E. Rignot, H. Seroussi, E. Larour, H. Ben Dhia, and D. Aubry (2010), Spatial patterns of basal drag inferred using control methods from a full-Stokes and simpler models for Pine Island Glacier, West Antarctica, *Geophys. Res. Lett.*, *37*, L14502, doi:10.1029/2010GL043853.
Morlighem, M., E. Rignot, H. Seroussi, E. Larour, H. Ben Dhia, and D. Aubry (2011), A mass conservation approach for mapping glacier ice thickness, *Geophys. Res. Lett.*, *38*, L19503, doi:10.1029/2011GL048659.
Nowicki, S. M. J., and D. J. Wingham (2008), Conditions for a steady ice sheet-ice shelf junction, *Earth Planet. Sci. Lett.*, *265*, 246–255.
Paterson, W. (1994), *The Physics of Glaciers*, 3rd ed., Pergamon, New York.
Pattyn, F. (1996), Numerical modelling of a fast-flowing outlet glacier: Experiments with different basal conditions, *Ann. Glaciol.*, *23*, 237–246.
Payne, A., A. Vieli, A. Shepherd, D. Wingham, and E. Rignot (2004), Recent dramatic thinning of largest West Antarctic ice stream triggered by oceans, *Geophys. Res. Lett.*, *31*, L23401, doi:10.1029/2004GL021284.
Pollard, D., and R. DeConto (2009), Modelling West Antarctica ice sheet growth and collapse through the past five million years, *Nature*, *458*, 329–332.
Rignot, E. (2008), Changes in West Antarctic ice stream dynamics observed with ALOS PALSAR data, *Geophys. Res. Lett.*, *35*, L12505, doi:10.1029/2008GL033365.
Rignot, E., M. Koppes, and I. Velicogna (2010), Rapid submarine melting of the calving faces of West Greenland glaciers, *Nat. Geosci.*, *3*, 187–191.
Schoof, C. (2007a), Marine ice-sheet dynamics. Part 1. The case of rapid sliding, *J. Fluid Mech.*, *573*, 27–55.
Schoof, C. (2007b), Ice sheet grounding line dynamics: Steady states, stability, and hysteresis, *J. Geophys. Res.*, *112*, F03S28, doi:10.1029/2006JF000664.
Seroussi, H., M. Morlighem, E. Rignot, E. Larour, D. Aubry, H. Ben Dhia, and S. S. Kristensen (2011), Ice flux divergence anomalies on 79north Glacier, Greenland, *Geophys. Res. Lett.*, *38*, L09501, doi:10.1029/2011GL047338.
Shapiro, N., and M. Ritzwoller (2004), Inferring surface heat flux distributions guided by a global seismic model: Particular application to Antarctica, *Earth Planet. Sci. Lett.*, *223*, 213–224.
Stokes, G. (1845), On the theories of internal friction of fluids in motion, *Trans. Cambridge Philos. Soc.*, *8*, 287–305.
Swiler, L. P., and G. D. Wyss (2004), A user's guide to Sandia's latin hypercube sampling software: LHS UNIX library/standalone version, *Tech. Rep. SAND2004-2439*, Sandia Natl. Lab., Albuquerque, New Mexico.
Utke, J., U. Naumann, M. Fagan, N. Tallent, M. Strout, P. Heimbach, C. Hill, and C. Wunsch (2008), Openad/f: A modular open-source tool for automatic differentiation of fortran codes, *ACM Trans. Math. Software*, *34*, 1–36.
Vaughan, D., et al. (2006), New boundary conditions for the West Antarctic Ice Sheet: Subglacial topography beneath Pine Island Glacier, *Geophys. Res. Lett.*, *33*, L09501, doi:10.1029/2005GL025588.
Velicogna, I. (2009), Increasing rates of ice mass loss from the Greenland and Antarctic ice sheets revealed by GRACE, *Geophys. Res. Lett.*, *36*, L19503, doi:10.1029/2009GL040222.
Vieli, A., and A. Payne (2003), Application of control methods for modelling the flow of Pine Island Glacier, West Antarctica, *Ann. Glaciol.*, *36*, 197–204.
Vieli, A., A. J. Payne, Z. Du, and A. Shepherd (2006), Numerical modelling and data assimilation of the Larsen B Ice Shelf, Antarctic Peninsula, *Phil. Trans R. Soc. A*, *364*, 1815–1839.

E. Larour, J. Schiermeier, and H. Seroussi, Jet Propulsion Laboratory, California Institute of Technology, 4800 Oak Grove Dr., Pasadena, CA 91109-8099, USA. (eric.larour@jpl.nasa.gov)

M. Morlighem and E. Rignot, Department of Earth System Science, University of California, Croul Hall, Irvine, CA 92697-3100, USA.

J. Paden, Center for Remote Sensing of Ice Sheets and EECS Department, University of Kansas, 2335 Irving Hill Rd., Lawrence, KS 66045-7612, USA.